Quench dynamics of edge states in a finite extended Su-Schrieffer-Heeger system

A. Ghosh,[1,2] A. M. Martin,[2] and S. Majumder[1]

[1]Indian Institute of Technology Kharagpur, Kharagpur 721302, West Bengal, India

[2]School of Physics, University of Melbourne, Victoria 3010, Australia

(Received 9 March 2023; accepted 8 August 2023; published 1 September 2023)

We examine the quench dynamics of an extended Su-Schrieffer-Heeger (SSH) model involving long-range hopping that can hold multiple topological phases. Using winding number diagrams to characterize the system's topological phases geometrically, it is shown that there can be multiple winding number transition paths for a quench between two topological phases. The dependence of the quench dynamics is studied in terms of the survival probability of the fermionic edge modes and postquench transport. For two quench paths between two topological regimes with the same initial and final topological phase, the survival probability of edge states is shown to be strongly dependent on the winding number transition path. This dependence is explained using energy band diagrams corresponding to the paths. Following this, the effect of the winding number transition path on transport is investigated. We find that the velocities of maximum transport channels varied along the winding number transition path. This variation depends on the path we choose, i.e., it increases or decreases depending upon the path. An analysis of the coefficient maps, energy spectrum, and spatial structure of the edge states of the final quench Hamiltonian provides an understanding of the path-dependent velocity variation phenomenon.

DOI: 10.1103/PhysRevE.108.034102

I. INTRODUCTION

Quench dynamics is an area of considerable interest in topological systems research [1–9]. Topics such as identifying topological features of dynamical quantum phase transitions [3,4], understanding how equilibrium topological quantum phases can be characterized in nonequilibrium scenarios [5], and investigating how information spreads in many-body systems after a quench [2,5] have been studied. For example, studies have shown that quasiparticle correlations spread when a system is quenched from deep inside a Mott insulating phase to the boundary of the superfluid phase [10,11], and research on XXZ Heisenberg chains has provided insights into how correlations spread in interacting many-particle systems [12].

One of the main thrusts in recent years has been to study the postquench fate of edge states in various topological settings, revealing some intriguing nonequilibrium physics. For instance, one-dimensional topological systems may contain isolated Majorana and fermionic modes, which exhibit fascinating behavior of the survival probabilities [1]. It has also been found that the postquench dynamical behavior of Majorana modes can also characterize the topological phase present in the system [2]. When quenched to quantum critical points, the survival probability of p-wave edge modes oscillates depending on the system configuration [6–8]. Quench dynamical studies are performed on the Kitaev one-dimensional superconductor [13] with p-wave pairing and one-dimensional dimerized Kitaev superconductors [14]. The dimerized Kitaev model can host several topological phases where the fermionic modes appear in the Su-Schrieffer-Heeger (SSH) -type Hamiltonian, which arises as a special case in the dimerized Kitaev model. The SSH system, being the simplest topological system [15,16], plays an important role in most of these quench studies, and there have also been several interesting works on its experimental realization [17–20]. Considering that SSH systems can host multiple higher topological states depending on the long-range interaction, there is a need to understand the dynamics of quench between these states.

In this paper, we study the SSH Hamiltonian in the presence of long-range hopping. For such a system, we geometrically show that it can host multiple topological phases. Based on the details of long-range hopping, the corresponding topological state is characterized by a winding number. Specifically, as the range of hopping increases, the maximum winding number the system can hold increases accordingly. We then investigate the quench dynamics of the system in terms of the survival probabilities of fermionic edge modes corresponding to the topological phase. We examine the survival probability of an edge mode, in a topological state, when the system is quenched to another topological state. Surprisingly, if we start in a well-defined edge state and quench via two different paths to a final topological state, the survival probability can be different, even though the topology of the system pre- and postquench is the same. Following that, we examine the spread of probability density over time on each site, and we observe the dynamical behavior of the quench, through "light-cone" diagrams. The slope of a channel in the light cones gives the velocity of that channel. Furthermore, we explain how the velocity of maximum transport varies along a quench path and how this variation is dependent on the path chosen.

The paper is organized as follows. In Sec. II, we introduce the extended SSH Hamiltonian with up to fourth-nearest-neighbor tunneling, enabling the possibility of having a maximum winding number of 4. In this section, using a geometric approach to mark the topological state, we introduce the concept of the path of winding number transition, and we show that there can be multiple paths of winding number transition possible corresponding to the same set of initial and final quench topologies. Section III presents our study of the dependence of quench dynamics of the fermionic edge modes on different paths of winding number transition corresponding to the same set of initial and final quenched topological states, with the results being explained via energy band diagrams corresponding to the quench paths. Following that, we demonstrate the variation in transport light cones corresponding to the quenches along these paths. By using coefficient maps of basis states, the energy spectrum of the final Hamiltonian, and spatial structuring of the edge states of the final Hamiltonian, we proceed to explain the dependence of velocity variation of the transport on the path. We conclude in Sec. IV with a review of our findings and possible future research avenues. A slightly different approach using phase diagrams is provided in Appendix A to demonstrate the topological phase map and the path of winding number transition of the problem discussed in the paper. We have included Appendix B to demonstrate that the same essential characteristics of path-dependent quench hold for a different configuration of the system involving different topological maps and paths.

II. EXTENDED SSH SYSTEM

In this work, we consider a dimensionless extended SSH Hamiltonian, i.e., a SSH system with long-range hopping present:

$$\hat{H} = v\sum_{m=1}^{N}|m,A\rangle\langle m,B| + w\sum_{m=1}^{N-1}|m+1,A\rangle\langle m,B| + \nu\sum_{m=1}^{N-2}|m+2,A\rangle\langle m,B| + \mu\sum_{m=1}^{N-3}|m+3,A\rangle\langle m,B| + \gamma\sum_{m=1}^{N-4}|m+4,A\rangle\langle m,B| + \text{H.c.}, \tag{1}$$

where v is the dimensionless intracellular hopping term, and w, ν, μ, and γ are the dimensionless intercellular first, second, third, and fourth nearest-neighbor hopping terms. These hopping terms respect the chiral symmetry, i.e., they represent hopping between two different sublattices (A and B in this case). This system can host several topological phases. We use winding number diagrams to keep track of the topological phases in a fashion similar to the works in [21,22]. To plot the winding number diagram for the system, we express $\hat{H}$ in terms of bulk momentum basis:

$$\hat{H}(k) = \langle k|\hat{H}|k\rangle = \sum_{\alpha,\beta\in\{A,B\}}\langle k,\alpha|\hat{H}|k,\beta\rangle|\alpha\rangle\langle\beta|, \tag{2}$$

where the plane-wave basis $|k\rangle$ is given by [15]

$$|k\rangle = \frac{1}{\sqrt{N}}\sum_{m=1}^{N}e^{imk}|m\rangle \tag{3}$$

and

$$\hat{H}(k) = \begin{bmatrix} 0 & a(k) \\ a^{\dagger}(k) & 0 \end{bmatrix}, \tag{4}$$

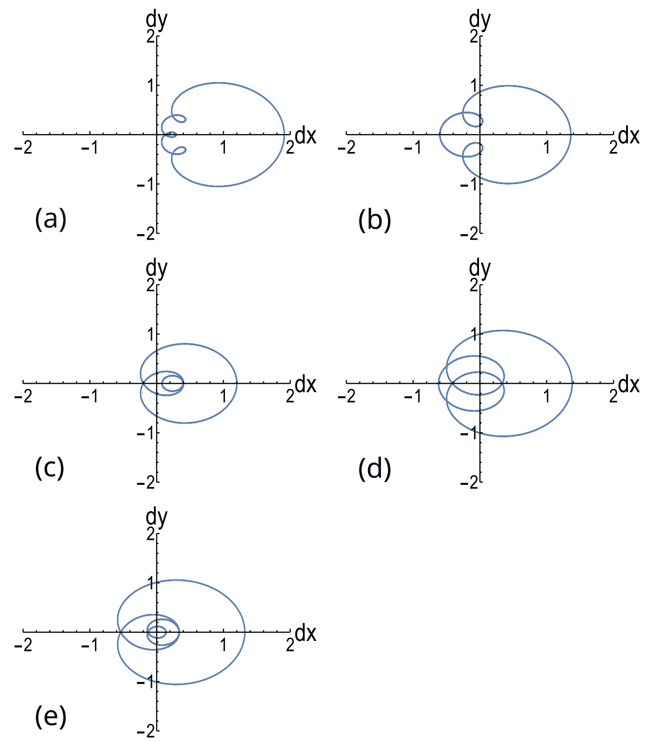

FIG. 1. The winding number representation in the d_x-d_y plane. Parts (a), (b), (c), (d), and (e) represent some possible topological states of the system with winding numbers 0, 1, 2, 3, and 4, respectively. The hopping parameters $v = 0.52$, $w = 0.54$, $\nu = 0.34$, $\mu = 0.27$, and $\gamma = 0.24$ in (a); $v = 0.1$, $w = 0.6$, $\nu = 0.28$, $\mu = 0.38$, and $\gamma = 0$ in (b); $v = 0.28$, $w = 0.2$, $\nu = 0.36$, $\mu = 0.36$, and $\gamma = 0$ in (c); $v = 0.1$, $w = 0.4$, $\nu = 0.28$, $\mu = 0.6$, and $\gamma = 0$ in (d); and $v = 0.1$, $w = 0.17$, $\nu = 0.25$, $\mu = 0.42$, and $\gamma = 0.38$ in (e).

where $a(k) = v + we^{ik} + \nu e^{i2k} + \mu e^{i3k} + \gamma e^{i4k}$. The matrix $\hat{H}(k)$ can be expressed in terms of Pauli matrices as

$$\hat{H}(k) = d_0\hat{\sigma}_0 + d_x\hat{\sigma}_x + d_y\hat{\sigma}_y + d_z\hat{\sigma}_z, \tag{5}$$

where, $\hat{\sigma}_0$, $\hat{\sigma}_x$, $\hat{\sigma}_y$, and $\hat{\sigma}_z$ are the Pauli matrices, and

$$d_x = v + w\cos(k) + \nu\cos(2k) + \mu\cos(3k) + \gamma\cos(4k), \tag{6}$$

$$d_y = w\sin(k) + \nu\sin(2k) + \mu\sin(3k) + \gamma\sin(4k), \tag{7}$$

$$d_0 = d_z = 0. \tag{8}$$

The winding number of the system is defined as the number of times the tip of the **d** vector encompasses the origin of (d_x, d_y)-space as k varies from 0 to 2π.

Figure 1 shows the winding number diagram corresponding to the topological phases possible in the system for different sets of parameters v, w, ν, μ, and γ. Additionally, Appendixes A and B present a phase diagrammatic approach to illustrate the topological phases present in an extended SSH system. It is important to note that the winding number diagrams presented in Fig. 1 are not unique for the winding numbers they are representing [15]. However, an important characteristic of the topological phases is that in a finite system, they host zero-energy edge states or fermionic edge modes in this case. In an ideal SSH system without any domains, the number of edge states is two times the winding number, a topological invariant.

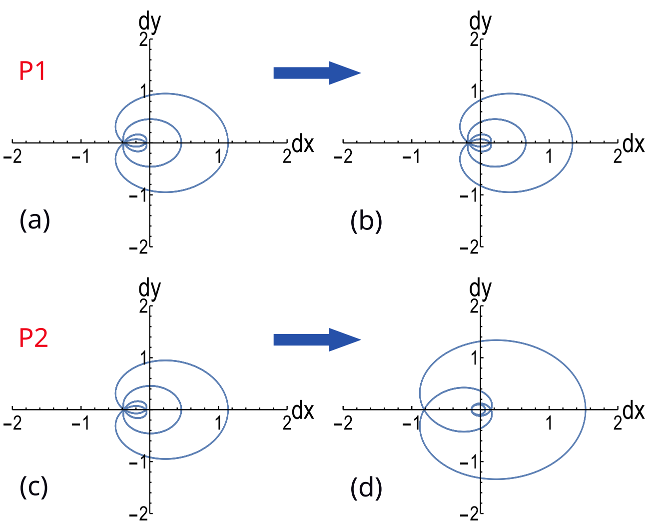

FIG. 2. Two possible paths for a transition from winding number 2 to winding number 4. $P1$ corresponds to a change in parameter v from 0 to 0.2, while keeping w, ν, μ, and γ fixed at 0.17, 0.43, 0.17, and 0.37, respectively. $P2$ corresponds to a change in parameter μ from 0.17 to 0.56, keeping the other parameters v, w, ν, and γ fixed at 0, 0.17, 0.43, and 0.37, respectively.

A. The path of winding number transition

In our study, the system is prepared in an initial state corresponding to an initial quench configuration with a particular topological phase characterized by the winding number, C_i. The system is then quenched to a final quench configuration, with a topological phase C_f.

Changing a parameter may change the winding number of the system, i.e., it may change from one winding number (say C_i) to another winding number (say C_f). It is also possible to bring about this same transition of winding number (C_i to C_f) by changing some other parameter. These ways of manifesting the same winding number transition constitute the *path of winding number transition*. In Fig. 2, we provide an example of such multiple paths by demonstrating two possible paths for the transition from the topological phase with $C_i = 2$ to $C_f = 4$. The first path ($P1$) corresponds to the change of the parameter v from 0 to 0.2, keeping the other parameters w, ν, μ, and γ fixed at 0.17, 0.43, 0.17, and 0.37, respectively. The second path ($P2$) corresponds to the change of the parameter μ from 0.17 to 0.56, keeping the other parameters v, w, ν, and γ fixed at 0, 0.17, 0.43, and 0.37, respectively. In each case, the topology of the initial and final states is the same. In Appendix A these paths are also discussed and represented in terms of a phase diagram in v and μ. In essence, the question we wish to ask and answer in Sec. III is the following. Suppose one starts in an edge state associated with a particular topology, and the system is quenched to another topological state. Does the winding number transition path impact the quench dynamics in terms of postquench transport and survival probability of an edge state? Put another way, is the quench dynamics of an edge state different for the paths $P1$ and $P2$ shown in Fig. 2? If it is different, what governs the properties of the survival probability of the edge state and postquench transport ("Light cones") through the system when quenching between two topological states?

Since we are investigating the dynamics of the quench along the paths corresponding to the various paths, it is necessary to investigate the topological phases that the system *passes* through along and past the quench. As an example, Fig. 3 and Fig. 10 in Appendix A denote the topological phases that the system passes through and past for the two paths $P1$ and $P2$, shown in Fig. 2. For the first path, the topological phases along the path are 2, 4, but if the v continues past 0.4, the system ends up in the topological state 0 (2-4-0). For the second path, it is 2, 4, and 3 (2-4-3), where, as μ continues past 0.6, the system ends up in the topological state 3. We will see in Sec. III that one of the most critical aspects of this characterization of a path (2-4) is where the topological phase for the quench is heading if we continue along the path of winding number transition: for $P1$ it is 0 and for $P2$ it is 3.

B. Survival probability of single-particle states

Before comparing different paths of winding number transition, we introduce the concept of survival probability for the initial state. With this in mind, consider a single-particle system defined by Hamiltonian $\hat{H}$, which is a function of a parameter χ_1 at $t < 0$. The single-particle states at this time are given by the Schrödinger's equation,

$$H(\chi_1)|\psi_i(\chi_1)\rangle = E_i(\chi_1)|\psi_i(\chi_1)\rangle. \tag{9}$$

At $t = 0$ a quench is performed, i.e., there is an instant change of parameter $\chi_1 \to \chi_2$. The eigenstates $|\psi_f\rangle$ corresponding to the new Hamiltonian with the parameter χ_2 are defined by Schrödinger's equation,

$$\hat{H}(\chi_2)|\psi_f(\chi_2)\rangle = E_f(\chi_2)|\psi_f(\chi_2)\rangle. \tag{10}$$

The time evolution of a single-particle state, $|\psi_i(\chi_1)\rangle$, postquench is given by

$$|\psi_i(t)\rangle = \sum_{f=1}^{N} e^{-iE_f(\chi_2)t}|\psi_f(\chi_2)\rangle\langle\psi_f(\chi_2)|\psi_i(\chi_1)\rangle, \tag{11}$$

where the sum is over the eigenstates associated with $\hat{H}(\chi_2)$. The likelihood of returning to our initial state at any time $t > 0$, also known as the survival probability of the initial state, is given by

$$P^i(t) = |\langle\psi_i(\chi_1)|\psi_i(t)\rangle|^2. \tag{12}$$

We will focus on this quantity in the first part of Sec. III to characterize the properties of a quench. More specifically, we will start with some well-defined edge state, characterized by the topology of the prequench system, and evaluate $P^i(t)$ postquench.

III. RESULT AND DISCUSSIONS

A. The dependence of survival probability on path

We know that edge states are topologically protected, and the number of edge states is determined by the winding number of the system. As we have discussed in previous sections, our system can host multiple topological phases, and there can be several paths possible for transition between the same set

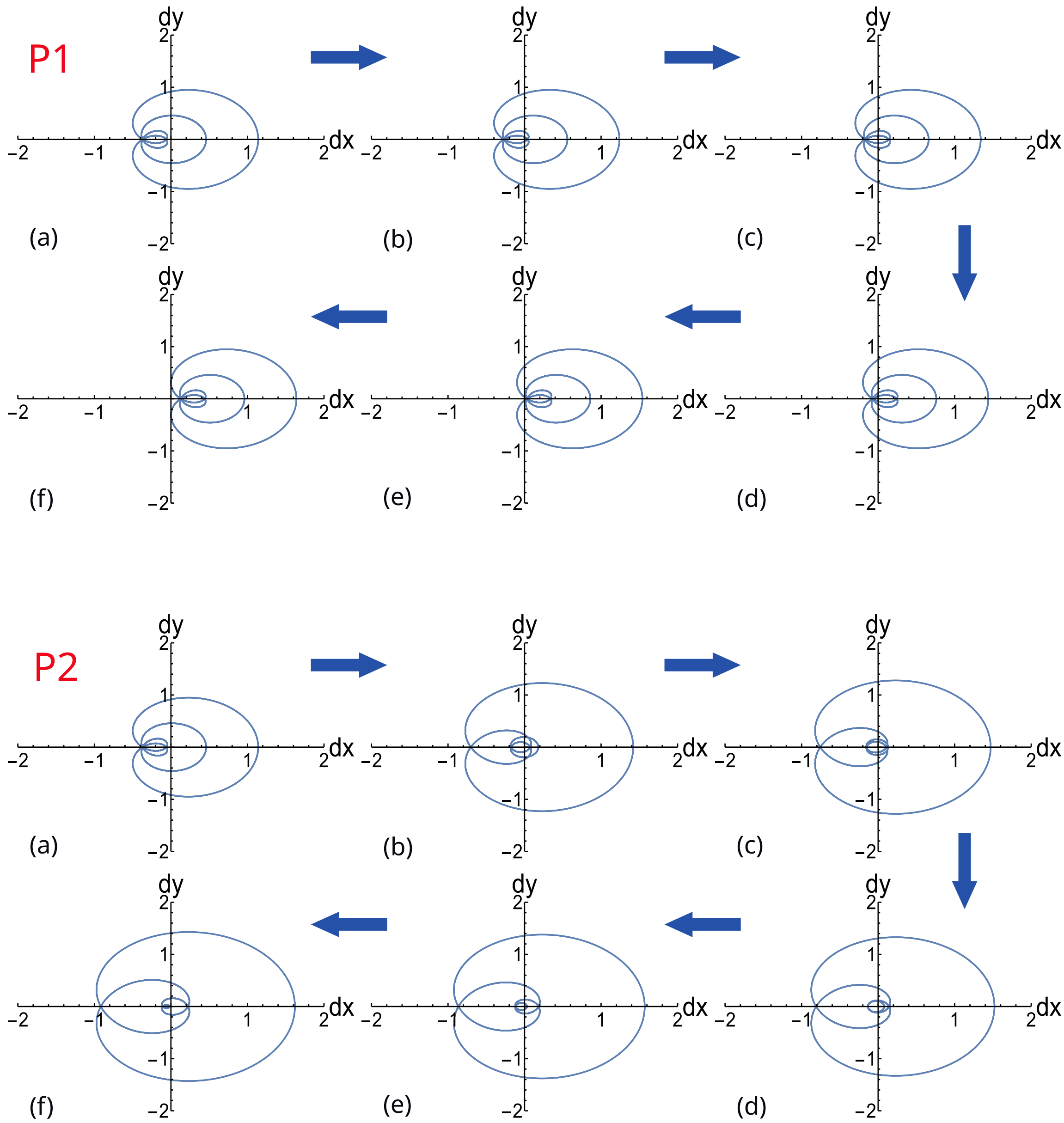

FIG. 3. The topological phases that the system takes along the two paths of winding number transition corresponding to the same initial winding number transition, from 2 to 4. In path $P1$, the parameter υ is gradually changed from 0 to 0.5, keeping other parameters w, ν, μ, and γ fixed at 0.17, 0.43, 0.17, and 0.37, respectively. Parts (a), (b), (c), (d), (e), and (f) of $P1$ correspond to the value of υ as 0.0, 0.1, 0.2, 0.3, 0.4, and 0.5, respectively. In $P1$, the topological phase flow is 2-4-0. In $P2$ the parameter μ is increased from 0.17 to 0.65 keeping other parameters υ, w, ν, and γ at 0, 0.17, 0.43, and 0.37, respectively. For $P2$, (a), (b), (c), (d), (e), and (f) correspond to the value of the parameter μ as 0.17, 0.45, 0.5, 0.55, 0.6, and 0.65, respectively. In $P2$, the topological phase flow is 2-4-3.

of winding numbers; see Fig. 2. Below we study the survival probabilities of edge states for quenches corresponding to different paths. As an example, we initially consider the standard SSH model with $\nu = \mu = \gamma = 0$, and our initial system defined by $\upsilon_i < w_i$, specifically $\upsilon_i = 0.2$ and $w_i = 0.5$, with $C_i = 1$. We then quench the system to $\upsilon_f > w_f$, specifically $\upsilon_f = 0.6$ and $w_f = 0.5$, with $C_f = 0$. For such a scenario, we consider a system with $N = 400$ sites, and the initial eigenstate is confined to the edge [see Fig. 4(a)], with dimensionless eigenenergy 0. After quenching, we see a dramatic drop off in the survival probability of the initial state [1,6]; see Fig. 4(b). The rationale for this rapid decay in survival probability is clear, i.e., we have quenched from a system $C_i = 1$, which supports an edge state, to a system $C_f = 0$, which does not.

In the following, we ask this question: if the postquench system supports edge states, $C_f > 0$, how will the survival probability of the initial edge state be affected, and how will the quench path impact it? As in Fig. 4, we consider a system with $N = 400$ sites. The initial eigenstate we consider is shown in Fig. 5(a), with $\upsilon_i = 0$, $w_i = 0.17$, $\nu_i = 0.43$, $\mu_i = 0.17$, and $\gamma_i = 0.37$, where $C_i = 2$. In Fig. 5(b), the survival probability for this initial state is plotted along the

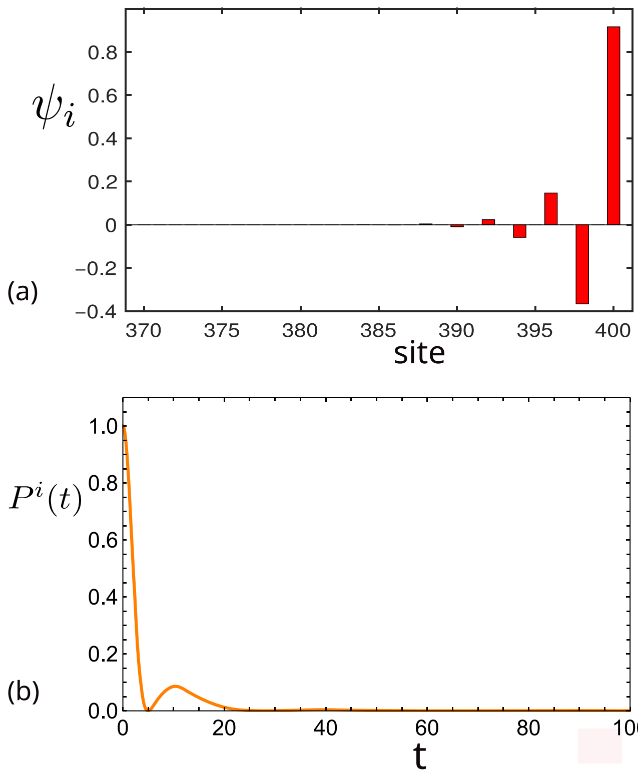

FIG. 4. (a) Edge state wave function in an $N = 400$ site system with $v_i = 0.2$ and $w_i = 0.5$. (b) Survival probability, $P^i(t)$, for $v_i = 0.2$, $w_i = 0.5$, $v_f = 0.6$, and $w_f = 0.5$, and the initial state is shown in (a).

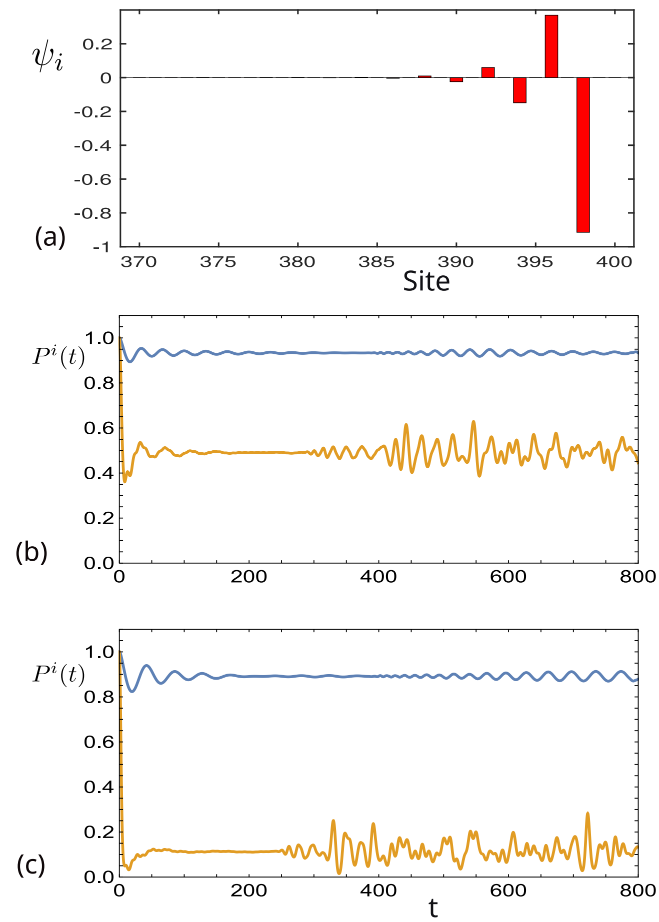

FIG. 5. (a) Edge state wave function in an $N = 400$ site system with $v_i = 0$, $w_i = 0.17$, $\nu_i = 0.43$, $\mu_i = 0.17$, and $\gamma_i = 0.37$, with $C_i = 2$. (b) Overlap probability, $P^i(t)$, for $v_f = 0.2$ (orange line) and $\mu_f = 0.56$ (blue line). (c) Overlap probability, $P^i(t)$, for $v_f = 0.3$ (orange line) and $\mu_f = 0.6$ (blue line). In (b) and (c), the initial state considered is the one shown in (a).

two quench paths shown in Fig. 2, specifically $v_f = 0.2$ (orange line) and $\mu_f = 0.56$ (blue line), noting that in each case $C_f = 4$.

From Fig. 5(b), it appears that quenching into a state that supports edge states enhances the survival of the prequench edge state. However, we note that for the quench to $v_f = 0.2$, the long-term behavior of the overlap with the initial state is just above 0.4. This contrasts with the quench to $\mu_f = 0.56$, where the long-term survival probability is just above 0.8. Examining this more closely, we consider quenches $v_f = 0.3$ (orange line) and $\mu_f = 0.6$ (blue line); see Fig. 5(c). The quenches here correspond to those closer to the boundary of $C_f = 4$. As can be seen in Fig. 3, if v_f is increased much further, C_f will eventually become 0, whereas if μ_f is increased much further, C_f will become 3. As can be seen across Figs. 5(b) and 5(c), the long-term survival probability for the quench in v is significantly less than for the quench in μ.

Other quenches show similar results, i.e., the survival probability of edge states is not only determined by the topology of the system they are quenched into, but also by the direction in which the quench is heading. For example, in Appendix B we have considered similar quench dynamics for a different system configuration with different paths. In the two examples here, we have to consider that the paths can be labeled as 2-4-0 (quenching v) and 2-4-3 (quenching μ). Writing the path labels in a more general sense as C_i-C_f-C_h, we can characterize the properties of the quench through examination of the energy band diagrams corresponding to the paths (Figs. 6 and 7).

Figure 6 shows the eigenenergies for path 2-4-0 as v is increased. As can be seen, in Fig. 6(b), the *zero-energy* states depart from their zero-energy character just after the first topological phase transition (2-4) as the parameter v increases. This departure results in a decrease in the survival probability for the quench 2-4-0, even though $C_f = 4$. However, the edge states maintain their character throughout the path $P2$ (2-4-3); see Fig. 7. This results in the survival probability of the edge state remaining relatively high after the quench.

From these results, it is clear that the quench dynamics of some edge states depends on the path chosen for the topological phase transition, even if the final topology of the system, C_f, is the same. For the example considered, we see that the quench can be characterized as either 2-4-0 or 2-4-3, and the latter path has a higher survival probability. From Figs. 6 and 7, we see that the details of the eigenenergy spectrum can provide insight into the survival probability. More generally, we have considered other quench paths and found that, for paths described by $C_i - C_f - C_h$, if two quenches are

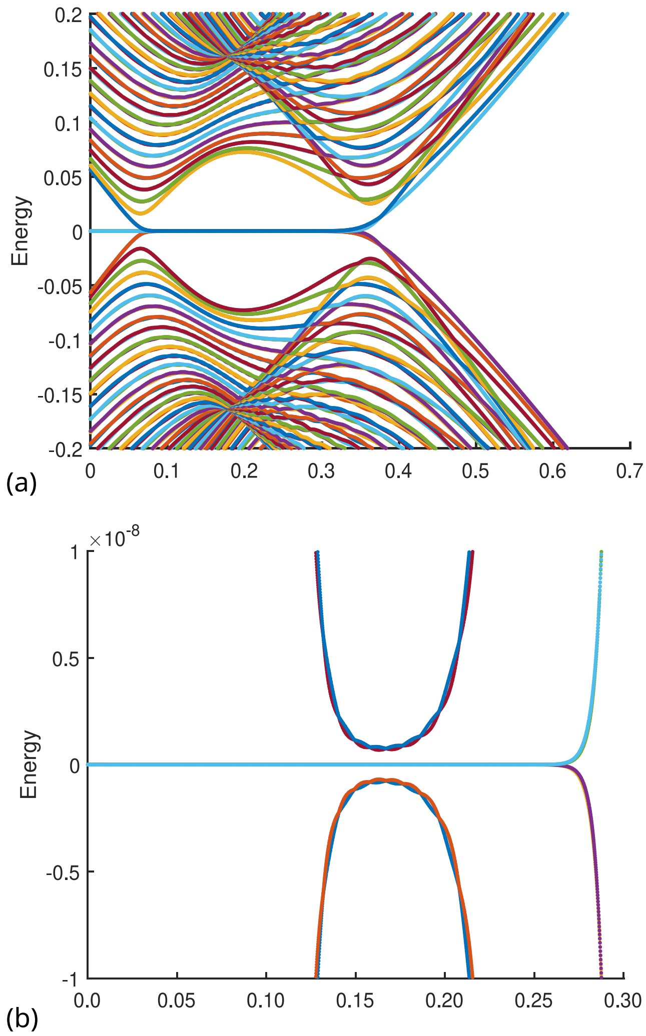

FIG. 6. (a) The eigenenergies of an $N = 400$ site system for $w = 0.17$, $\nu = 0.43$, $\mu = 0.17$, and $\gamma = 0.37$ as a function of v. (b) A zoomed-in plot of (a) focusing on energies close to zero.

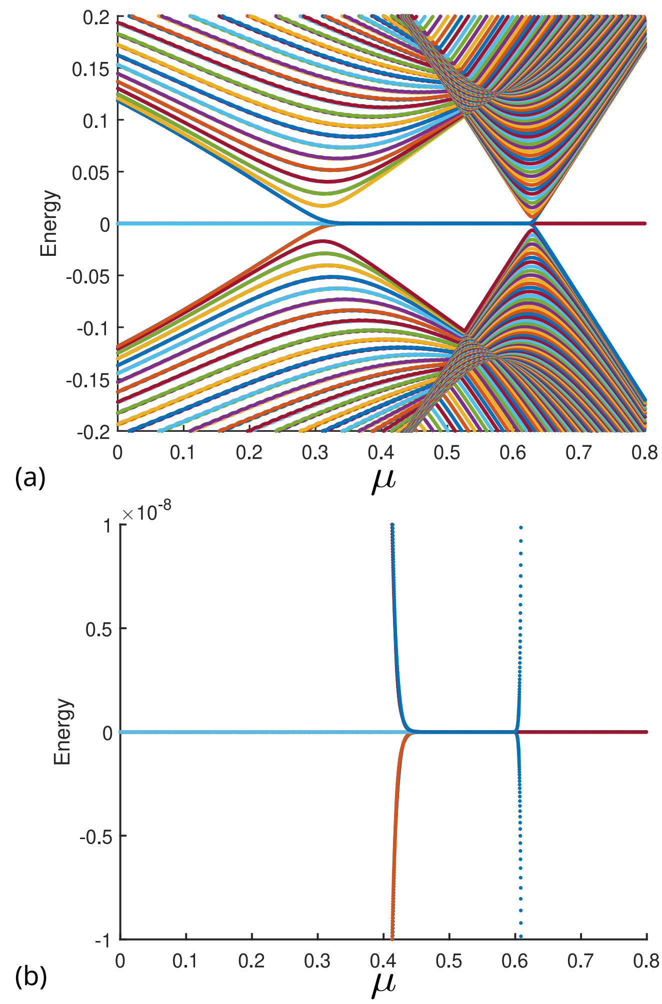

FIG. 7. (a) The eigenenergies of an $N = 400$ site system for $v = 0$, $w = 0.17$, $\nu = 0.43$, and $\gamma = 0.37$ as a function of μ. (b) A zoomed-in plot of (a) focusing on energies close to zero.

considered starting at the same initial state and having the same C_f, the survival probability will be larger if $C_h \geqslant C_i$ as compared to the case where $C_h < C_i$. Appendix B provides such an example.

In Fig. 5, one can observe a pattern of the survival probability, which is related to interference. Specifically, in all cases, the survival probability, on short timescales, exhibits a dip. This is followed by a regime where the survival probability is constant, and then comes a regime of ripples. We find that the timescale on which the ripples occur scales with system size. This can be understood by considering the transport of the probability density, with the ripples arising as a result of interference between probability density waves present at the edge and the reflected wave from the other edge. The timescale for the onset of this interference increases linearly with system size. The time of the arrival of the ripples in the survival probability is different for the two paths, and also, it is slightly different for Figs. 5(b) and 5(c) corresponding to the paths. The underlying physics is related to the nonequilibrium transport of the edge states corresponding to the paths, which will be discussed in detail below.

B. Variation of transport velocity with the type of path

The discussion in the previous subsection suggests that the postquench dynamics are associated with the transport of the edge states across the system. Below we visualize this transport using light-cone diagrams, i.e., a diagram that plots probability density $[n_i(t) = \langle\psi_i(t)|\psi_i(t)\rangle]$ on each site with respect to time. Figure 8 characterizes the transport of the edge state for quenches along $P1$ corresponding to the values $v_f = 0.1$ and 0.3 in (a) and (b), respectively, with $v_i = 0$, whereas Figs. 8(c) and 8(d) correspond to the transport of the edge state for quenches along $P2$ corresponding to the values $\mu_f = 0.39$ and 0.59, respectively, with $\mu_i = 0.17$. Comparing Figs. 8(a) with 8(b), and Figs. 8(c) with 8(d), it can be observed that there is a change in the velocity of the channels through which the maximum transport is taking place as the final quench configuration is moved along $P1$ and $P2$, respectively. This velocity variation is quantitatively different for the two paths of the quench. By comparing Figs. 8(a) with 8(b), we see that the velocity of the maximum transport increases for $P1$. More generally, we find that the velocity of maximum transport channels increases for paths that characterize a decaying

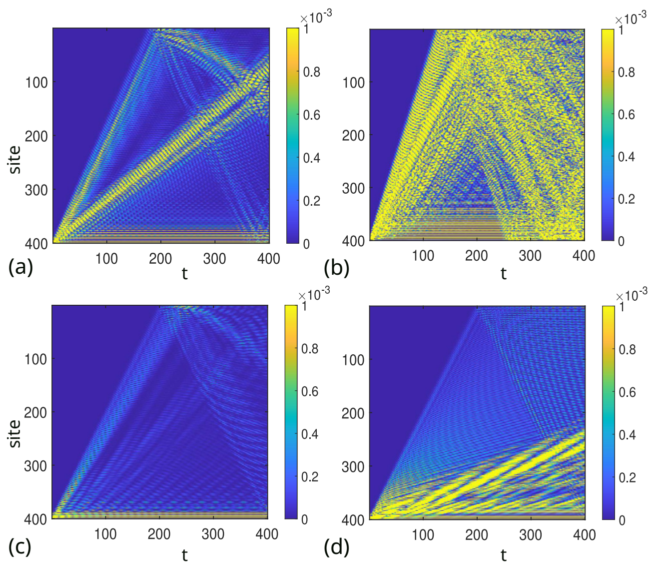

FIG. 8. Four light-cone diagrams for quenches of v from $v_i = 0$ to (a) $v_f = 0.1$ and (b) $v_f = 0.3$ with w, ν, μ, and γ fixed at 0.17, 0.43, 0.17, and 0.37, respectively, and quenches of μ from $\mu_i = 0.17$ to (c) $\mu_f = 0.39$ and (d) $\mu_f = 0.59$ with v, w, ν, and γ fixed at 0, 0.17, 0.43, and 0.37, respectively. Each light-cone diagram plots the probability density $[n_i(t) = \langle \psi_i(t)|\psi_i(t)\rangle]$ on each site i (y-axis) as a function of time (x-axis).

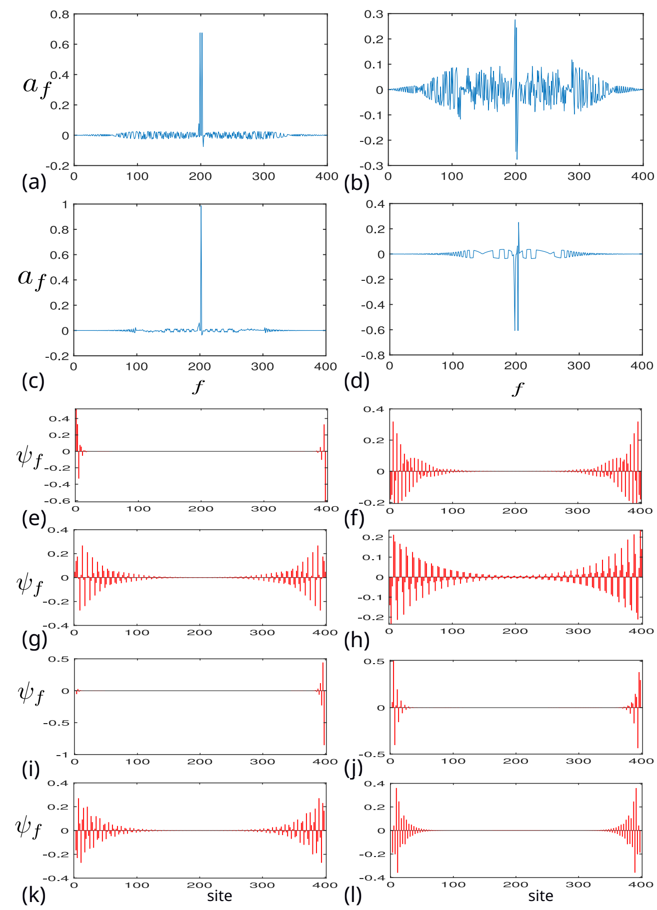

FIG. 9. In this figure, (a), (b), (c), and (d) are the plots of the coefficient $a_f = \langle \psi_f(\chi_2)|\psi_i(\chi_1)\rangle$ against the indices f corresponding to $v_f = 0.1$, $v_f = 0.3$ of $P1$ and $\mu_f = 0.39$, $\mu_f = 0.59$ of $P2$, respectively. Parts (e),(g) and (f),(h) correspond to edge states of $v_f = 0.1$ and 0.3 along $P1$, respectively, with (e),(f) having the lowest order of energies and (g),(h) having relatively higher orders of energies in their respective Hamiltonians. Parts (i),(k) and (j),(l) correspond to edge states of $\mu_f = 0.39$ and 0.59 along $P2$, respectively, with (i),(j) having the lowest order of energies and (k),(l) having a relatively higher order of energies in their respective Hamiltonians. The central peaks from 197 to 204 in the coefficient plots correspond to the high overlap with some of the edge states of the final Hamiltonian. The delocalization in the edge states along $P1$ is clear if we compare (e),(g) with (f),(h). Similarly, the localization in the transport contributing edge state along $P2$ is apparent if we compare (k) with (l).

survival probability of edge states, whereas for the path that does not characterize a decaying survival probability of edge state ($P2$), the velocity variation of the channel of maximum transport is from high to low as we move along the quench path, as can be seen when comparing Figs. 8(c) with 8(d). Close examination of Fig. 8(a) reveals that there are two dominant channels through which the transport takes place. One of these channels corresponds to a relatively high velocity (lower intensity) as compared to the other, which corresponds to a lower velocity (higher intensity). As the final quench configuration is moved along the path $P1$, the velocity corresponding to both of the channels increases. Also, during the journey along path $P1$, the velocities tend to be closer in magnitude, and the intensity of the faster velocity channel increases slightly. On the other hand, Fig. 8(c) demonstrates that there is very low transport in total. As the final quench configuration is moved along path $P2$, there is an increased transport along a much lower velocity channel than the previous configuration. This phenomenon has also been demonstrated in Appendix B for a different system configuration with different paths.

To explain the velocity variation phenomenon, we explore the correspondence between the components of Eq. (11) and the light cones depicted in Fig. 8. We examine, in Fig. 9, the change in the coefficients, $a_f = \langle \psi_f(\chi_2)|\psi_i(\chi_1)\rangle$, of the basis vectors in the expression for the evolving state in Eq. (11), and the spatial structure of the edge states as we move along the path, i.e., the localization and delocalization of the edge states. The coefficient a_f is dependent on the spatial structure of the eigenstates of the final Hamiltonian. Since the summation in Eq. (11) is over all the eigenstates of the final Hamiltonian, both the edge states and the bulk states contribute to the transport. The coefficient of terms in the summation dictates its weight and hence corresponds to the intensity of the channel. The energies of states, along with the time, come as a phase factor in the expression and hence they contribute to the velocity of transport. Figures 9(a)–9(d) correspond to the coefficients for $v_f = 0.1$, $v_f = 0.3$ of path $P1$ and $\mu_f = 0.39$, $\mu_f = 0.59$ of path $P2$, respectively. The coefficients from 197 to 204 in Figs. 9(a)–9(d) correspond to the edge states and the rest to the bulk states. The peaks in the central region of these figures come from the strong overlap of the initial edge state with the edges states in the postquench Hamiltonian. In Figs. 9(a)–9(d), the highest peaks correspond to the edge states with the lowest order of energy [as shown in Figs. 9(e), 9(f), 9(i), and 9(j) for $v_f = 0.1$ and 0.3 ($P1$), and $\mu_f = 0.39$

and 0.59 ($P2$), respectively], and these contribute to the static horizontal lines at the bottom of the light-cone diagrams. It may be observed that the spread of the horizontal lines toward the center of the wire is more in Fig. 8(b) than in Fig. 8(a), and the reason for this may be attributed to the fact that there is a delocalization in the edge states as we move from $v = 0.1$ to 0.3. The delocalization is clearly visible if we compare Figs. 9(e) and 9(g) with Figs. 9(f) and 9(h), which corresponds to $v = 0.1$ and 0.3 of $P1$, respectively. For all of the cases, the next highest contribution comes from the edge states whose energies are close to zero but are orders of magnitude higher than that of the stationary edge states, and these correspond to the slow velocity channel in the light cones of Fig. 8. The energies of these states increase as we move along the paths, and this results in an increase in the velocity of the slower velocity channel. This result is more prominent in Figs. 8(a) and 8(b) as the corresponding coefficients in this path $P1$ are higher than in $P2$. As we move along the path $P2$ [Figs. 8(c) and 8(d)], it might appear that the velocity of the channel of most transport decreases, as shown in Figs. 8(c) and 8(d), however it appears so because the coefficients of the lower velocity channel were initially very low and it increased as we moved along the path, resulting in significant transport through the low-velocity channel, making the lower velocity channel most intense. It is important to note that the coefficient corresponding to the lower velocity channel increases along path $P2$ due to the localization of the edge states. Due to localization, the amplitude near the edges increases, increasing the coefficient. The coefficients corresponding to the bulk states in Fig. 9(b) are much higher when compared to the coefficients in Fig. 9(a). This is the reason that the intensity of the higher velocity channel in the former is much higher than that of the latter. The velocity of the higher velocity channel also increases as we move along a path, and this is because of the increase in the bulk state energies. As we move along the path $P2$, the bulk state energies increase as well, but there is localization in the edge states, leading to less contribution to transport, and so the velocity and magnitude of the higher velocity channel do not increase significantly.

IV. SUMMARY AND CONCLUSIONS

By analyzing the topological phases of the extended SSH model using winding number diagrams, we have shown that there can be multiple paths of winding number transition possible for a quench between two topological phases. By studying the path dependence of quench dynamics in terms of fermionic edge-state survival probability, we found that it is possible to classify the survival probability in terms of three general parameters: (i) the prequench winding number (C_i), (ii) the postquench winding number (C_f), and (iii) the winding number of where the quench is heading (C_h). In general, we find that for a system characterized by $C_i - C_f - C_h$ if two quenches are considered with the same C_i and C_f, the survival probability for some of the fermionic edge-state will be greater for the quench with $C_h \geqslant C_i$ as compared to the case where $C_h < C_i$. This classification of the robustness of edge states when quenching between two topological regimes has only been tested within this model, and further work is required to test this concept more broadly. We then studied postquench dynamics through the use of light cone diagrams associated with probability density. Focusing on the example paths we have considered, we found that the velocities of the channels of most transport vary along the path of the winding number transition. This variation depends on the path we choose, i.e., for the path characterizing a decaying (stable) survival probability, the velocity corresponding to the most transport increases (decreases) along the path. The velocity variation phenomenon is explained by analyzing the coefficient plots, the energy spectrum of the final Hamiltonian, and the spatial structure of the edge states of the final Hamiltonian.

This study is limited to single quenches, but if multiple quenches are to be considered, there can be interesting questions. As an example, for two fixed points on a phase diagram (see Fig. 10 in Appendix A for example), there can be multiple sequences of quenches leading from one to another; how will different sequences behave in terms of edge state survival probability?

ACKNOWLEDGMENTS

We want to express our great appreciation to our group members at the University of Melbourne and IIT Kharagpur for their valuable and constructive suggestions during the planning and development of this research work. Their willingness to participate eagerly in the discussion sessions is greatly appreciated. This project was supported by an Institute fellowship from IIT Kharagpur, the government of India, and the N.D. Goldsworthy scholarship from the University of Melbourne, Australia. We are deeply thankful to them for supporting this project.

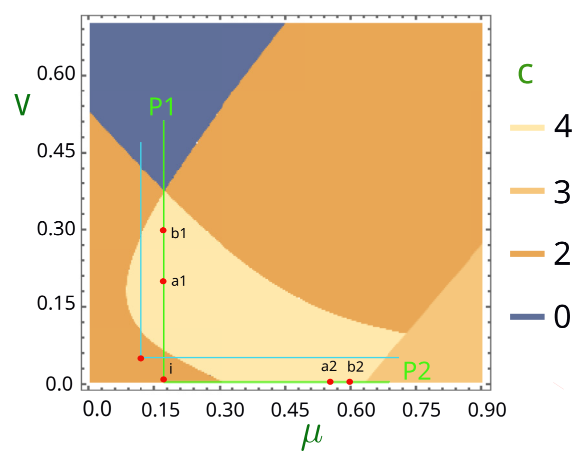

FIG. 10. This figure shows the topological map of the system with respect to the change in parameters v and μ, keeping the other parameters w, ν, and γ fixed at 0.17, 0.43, and 0.37, respectively. The color panel indicated by the letter C denotes the topological phases present in the system. The paths of winding number transition corresponding to $C_i = 2$ and $C_f = 4$, labeled as $P1$ and $P2$, are shown as green lines originating from the point in $C_i = 2$, labeled as i. Points $a1$ and $b1$ are along path $P1$, and points $a2$ and $b2$ are along path $P2$, and these particular points are used in the main paper to demonstrate the contrasting survival probabilities for the two paths. For this set of fixed w, ν, and γ, there can be other sets of paths possible, and one of those sets is shown using the arctic blue lines.

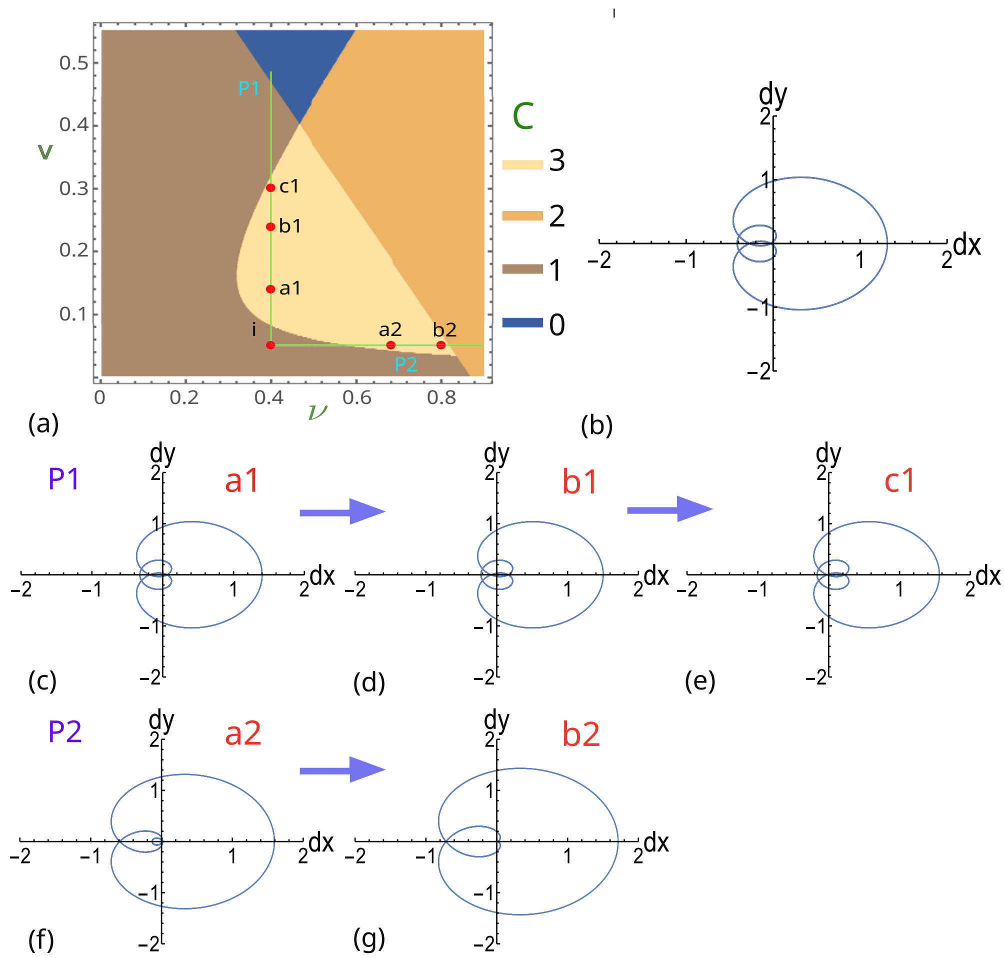

FIG. 11. This figure consists of a topological phase diagram of the system and geometrical representations of the topological state as the system progresses through the paths $P1$ and $P2$. Part (a) represents the topological phase diagram with variations in υ and ν with the values of parameters w and μ fixed at 0.463 and 0.4, respectively. The paths of winding number transition from $C_i = 1$ to $C_f = 3$ is shown with two green lines starting from the initial point i with $C_i = 1$. Points $a1$, $b1$, and $c1$ are along the path $P1$, and points $a2$ and $b2$ are along the path $P2$. Part (b) is the geometrical representation of the topological state of the initial point i with $C_i = 1$. Parts (c), (d), and (e) are the winding number diagrams of the points $a1$, $b1$, and $c1$ along $P1$. Similarly, parts (f) and (g) are the geometrical representations of the topological phases of the points $a2$ and $b2$ along path $P2$.

APPENDIX A: PHASE DIAGRAMMATIC DEMONSTRATION OF THE TOPOLOGICAL PHASES AND QUENCH DISCUSSED IN THE PAPER

As discussed in the main section of the paper, multiple transition paths can be possible to change the topological phase from an initial state C_i to a final state C_f. We have studied the dependence of quench dynamics on the path, i.e., in the particular case considered, topological phase was changed from $C_i = 2$ to $C_f = 4$ by either by changing the parameter υ keeping w, ν, μ, and γ fixed, or changing the parameter μ keeping υ, w, ν, and γ fixed.

In momentum space, the Hamiltonian, Eq. (4), is a two-level system and the winding number is given by [15]

$$C = \frac{1}{2\pi i}\int_0^{2\pi} \frac{d}{dk} \log{(a(k))} dk. \tag{A1}$$

Figure 10 represents the phase diagram in υ and μ keeping all the other parameters fixed. In this diagram, different colored regions show the topological phases possible for the (υ, μ) combination corresponding to fixed w, ν, and γ. The paths $P1$ and $P2$ have been marked. Path $P1$ consists of quench from point "i" in the topological phase with $C_i = 2$ to points like $a1$ and $b1$ corresponding to the topological phase $C_f = 4$, and path $P2$ consists of quench from the same point "i"$(C_i = 2)$ to points $a2$ and $b2$ with topological phase $C_f = 4$. There can be other possible paths, with the same $C_i - C_f$, corresponding to this configuration (of w, ν, and γ) as demonstrated in Fig. 10. It is important to note that the illustrated phase diagram is for the particular set of w, ν, and γ, and there can be many such diagrams corresponding to different combinations of w, ν, and γ. As mentioned in the paper, $P1$ with $C_h < C_i$ will characterize some edge states with decaying survival probability and increasing transport velocity along the path. It may also show stable survival probability and decreasing velocity depending on the initial edge state that we are considering. $P2$ will have all edge states with stable survival probability and decreasing velocity.

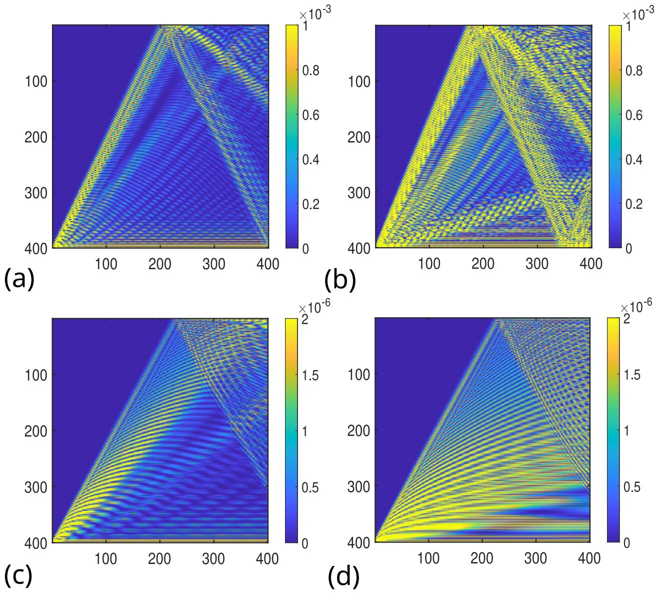

FIG. 12. This figure shows four light cone diagrams, i.e., the probability density on each site as a function of time. Parts (a) and (b) correspond to the quench along path $P1$ where the C_f is the points $a1$ and $b1$, respectively. Similarly, parts (c) and (d) correspond to the quench along path $P2$ where the C_f is the points $a2$ and $b2$, respectively.

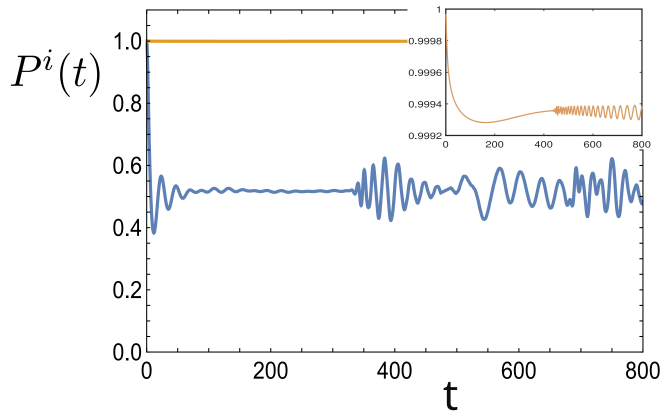

FIG. 13. This figure demonstrates the contrasting nature of the survival probability [$P^i(t)$] vs time (t) behavior for the two paths $P1$ and $P2$. The orange line corresponds to a quench along path $P2$, which is obtained by varying ν from 0.4 to 0.8, keeping v, w, and μ fixed at 0.05, 0.463, and 0.4, respectively (from point i to $b2$). The blue line represents the survival probability of path $P1$, which is obtained by varying v from 0.05 to 0.24, keeping w, ν, and μ fixed at 0.463, 0.4, and 0.4, respectively (from point i to $b1$). Although the orange line looks straight, a closer inspection (see the inset) reveals the onset of waves in the plot.

APPENDIX B: AN ADDITIONAL EXAMPLE WITH THREE NEAREST NEIGHBORS

In the main paper, we have considered a system with up to fourth-nearest-neighbor hopping, whereas below we consider a system with up to third-nearest-neighbor hopping, i.e., throughout this Appendix, $\gamma = 0$. Here, we will demonstrate that the same essential results of the quench dynamics study hold for the present case, i.e., the survival probability and the velocity variation are characterized by the path of winding number transition. The longest next-nearest interaction determines the highest winding number (or the maximum number of edge states) the system can host. These extended terms make it possible to study the same quench ($C_i - C_f$) through multiple paths of winding number transition. Figure 11 shows the phase diagram corresponding to the variation in the parameters v and ν, keeping the other parameters w and μ fixed at 0.463 and 0.4, respectively. As can be seen, there are three topologically nontrivial phases present in the system. The initial state is assumed to be an edge state corresponding to the topological state "i" with $C_i = 1$ in the phase diagram. Now, we wish to study the quench dynamics for the quench from $C_i = 1$ to $C_f = 3$. There are two ways to achieve this for single parameter quenching, which we call the path of winding transition. Path $P1$ constitutes changing v and keeping w, ν, and μ fixed, whereas $P2$ constitutes changing ν and keeping v, w, and μ constant. The phase diagram [Fig. 11(a)] shows these two paths, and we have also provided the winding number diagrams [Figs. 11(c), 11(d), and 11(e), and Figs. 11(f) and 11(g)] corresponding to the points in the paths to illustrate geometrically how the topological phase evolves along the paths for each path starting at Fig. 11(b).

It is evident from Fig. 11(a) that for the path $P1$, the topological phases acquired by the system are in the order 1-3-1-0, with $C_h = 0$ ($< C_i = 1$), whereas for path $P2$, the topological phases developed are in the order 1-3-2, with $C_h = 2$ ($> C_i = 1$). As discussed in the main section of the paper, path $P1$ should characterize some edge states with decaying survival probabilities and increasing transport velocity along the path. Also, path $P2$ should have all the edge states with stable survival probabilities and decreasing transport velocity along the path. The points on path $P1$ where we study the quench dynamics ($C_i - C_f$) are $a1$, $b1$, and $c1$, which correspond to the topological phase with $C_f = 3$. Similarly, the sampling points along $P2$ are $a2$ and $b2$ with $C_f = 3$. It is important to note that we have chosen this particular configuration of parameters to demonstrate the path dependence of quench, and there can be many such phase diagrams possible corresponding to the different values of w and μ.

Figure 12 is the light cone diagram for this system representing the variation probability density with respect to time. This quench configuration confirms the same velocity variation phenomenon (as discussed in the main paper), i.e., along the path $P1$ [refer to Figs. 12(a) and 12(b)], the velocity of maximum transport increases, while along the path $P2$ [refer to Figs. 12(c) and 12(d)], it decreases. Figure 12(a) seems to have a single channel transport as compared to Fig. 12(b) because the counterpart of the slower velocity channel in Fig. 12(b) has the corresponding velocity close to zero in the case of Fig. 12(a), and the intensity was also negligible in Fig. 12(a).

Figure 13 illustrates the characteristics of the path of winding number transition in terms of survival probability. It confirms the characteristic pattern of decaying (stable) survival probability depending upon whether $C_h < (>) C_i$. The plot in blue represents the survival probability of an edge state with time for the quench with the initial topological state at "i" in the phase diagram [Fig. 11(a)] to the final state $b1$, and the orange line corresponds to a quench from the same initial point to the final point $b2$.

[1] P. D. Sacramento, Edge mode dynamics of quenched topological wires, Phys. Rev. E **93**, 062117 (2016).

[2] Y. Wang, Detecting topological phases via survival probabilities of edge majorana fermions, Phys. Rev. E **98**, 042128 (2018).

[3] J. C. Budich and M. Heyl, Dynamical topological order parameters far from equilibrium, Phys. Rev. B **93**, 085416 (2016).

[4] C. Yang, L. Li, and S. Chen, Dynamical topological invariant after a quantum quench, Phys. Rev. B **97**, 060304(R) (2018).

[5] L. Zhang, L. Zhang, S. Niu, and X.-J. Liu, Dynamical classification of topological quantum phases, Sci. Bull. **63**, 1385 (2018).

[6] A. Rajak and A. Dutta, Survival probability of an edge majorana in a one-dimensional p-wave superconducting chain under sudden quenching of parameters, Phys. Rev. E **89**, 042125 (2014).

[7] A. Rajak and T. Nag, Survival probability in a quenched majorana chain with an impurity, Phys. Rev. E **96**, 022136 (2017).

[8] P. D. Sacramento, Fate of majorana fermions and chern numbers after a quantum quench, Phys. Rev. E **90**, 032138 (2014).

[9] M. Jangjan, L. E. F. F. Torres, and M. V. Hosseini, Floquet topological phase transitions in a periodically quenched dimer, Phys. Rev. B **106**, 224306 (2022).

[10] M. Cheneau, P. Barmettler, D. Poletti, M. Endres, P. Schauß, T. Fukuhara, C. Gross, I. Bloch, C. Kollath, and S. Kuhr, Light-cone-like spreading of correlations in a quantum many-body system, Nature (London) **481**, 484 (2012).

[11] J.-S. Bernier, R. Tan, L. Bonnes, C. Guo, D. Poletti, and C. Kollath, Light-Cone and Diffusive Propagation of Correlations in a Many-Body Dissipative System, Phys. Rev. Lett. **120**, 020401 (2018).

[12] L. Bonnes, F. H. L. Essler, and A. M. Läuchli, "Light-Cone" Dynamics After Quantum Quenches in Spin Chains, Phys. Rev. Lett. **113**, 187203 (2014).

[13] A. Y. Kitaev, Unpaired majorana fermions in quantum wires, Phys. Usp. **44**, 131 (2001).

[14] R. Wakatsuki, M. Ezawa, Y. Tanaka, and N. Nagaosa, Fermion fractionalization to majorana fermions in a dimerized kitaev superconductor, Phys. Rev. B **90**, 014505 (2014).

[15] J. K. Asbóth, L. Oroszlány, and A. Pályi, A short course on topological insulators, Lect. Notes Phys. **919**, 166 (2016).

[16] W. P. Su, J. R. Schrieffer, and A. J. Heeger, Solitons in Polyacetylene, Phys. Rev. Lett. **42**, 1698 (1979).

[17] M. Kiczynski, S. K. Gorman, H. Geng, M. B. Donnelly, Y. Chung, Y. He, J. G. Keizer, and M. Y. Simmons, Engineering topological states in atom-based semiconductor quantum dots, Nature (London) **606**, 694 (2022).

[18] E. J. Meier, F. A. An, and B. Gadway, Observation of the topological soliton state in the Su–Schrieffer–Heeger model, Nat. Commun. **7**, 13986 (2016).

[19] S. Liu, H. Yin, D. J. Singh, and P.-F. Liu, Ta_4SiTe_4: A possible one-dimensional topological insulator, Phys. Rev. B **105**, 195419 (2022).

[20] N. R. Cooper, J. Dalibard, and I. B. Spielman, Topological bands for ultracold atoms, Rev. Mod. Phys. **91**, 015005 (2019).

[21] G. Zhang and Z. Song, Topological Characterization of Extended Quantum Ising Models, Phys. Rev. Lett. **115**, 177204 (2015).

[22] C. Yin, H. Jiang, L. Li, R. Lü, and S. Chen, Geometrical meaning of winding number and its characterization of topological phases in one-dimensional chiral non-hermitian systems, Phys. Rev. A **97**, 052115 (2018).